Havenith et al. Geoenvironmental Disasters (2015) 2:11
DOI 10.1186/s40677-015-0021-x

Geoenvironmental Disasters
a SpringerOpen Journal

RESEARCH ARTICLE Open Access

The Kambarata 2 blast-fill dam, Kyrgyz Republic: blast event, geophysical monitoring and dam structure modelling

Hans-Balder Havenith[1*], Isakbek Torgoev[2], Almaz Torgoev[1,2], Alexander Strom[3], Yuan Xu[4] and Tomas Fernandez-Steeger[5]

Abstract

Background: The blast- and earth-fill dam of the Kambarata 2 hydropower station is situated in the seismically active Central Tien Shan region of the Kyrgyz Republic. More than 70% of the dam volume was produced during a blast event on December 22, 2009. In 2010–2011, dam construction was completed after earth filling on top of the blasted material and installing concrete and clay screens together with bentonite grouts. A geophysical survey had been completed in 2012–2013, mainly to monitor the resistivities inside the dam.

Results: The geophysical survey completed on the Kambarata 2 dam site showed lower resistivity zones in the earth fill and relatively higher resistivities in the blast-fill material. Topographic, geophysical and piezometric inputs had been compiled within a 3D geomodel constructed with GOCAD software. This model was compared with the design structure of the dam in order to define the upper limits of the underlying alluvium, the deposited blast fill, earth fill and top gravel materials (represented by the dam surface). The central cross-section of this model was extrapolated over the full length of the main dam profile.

Conclusions: On the basis of a calibrated hydrogeological model and known geomechanical properties of the materials, dam stability calculations were completed for different scenarios considering different reservoir levels and varying seismic conditions. Some of these scenarios indicated a critical vulnerability of the dam, e.g., if impacted by a horizontal seismic acceleration of Ah = 0.3 g and a vertical seismic acceleration Av = 0.15 g, with an estimated return period of 475 years.

As a general conclusion, it was noted that this case study can be used as an example for surveys on much larger natural – landslide or moraine – dams. A series of geophysical methods (e.g., electrical and electro-magnetic techniques, seismic and microseismic measurements) can be applied to investigate even very deep dam structures. These methods have the advantage over classical direct prospecting techniques, such as drilling, of using equipment that is much lighter and thus more easily transportable and applicable in difficult terrain. Furthermore, they can provide continuous information over wider areas. This specific application to a blast-fill dam allows us to better outline the strengths and weaknesses of the exploration types and geomodels as a series of investigated parameters can be verified more easily than for natural dams.

Keywords: Hydropower plant; Artificial dam; Blast event; Natural blockage; Electrical resistivity tomography; 3D geomodel; Hydro-geomechanical modelling

* Correspondence: HB.Havenith@ulg.ac.be
[1]Department of Geology, University of Liege, Liege, Belgium
Full list of author information is available at the end of the article

Background

Natural blockages formed by bedrock landslides may persist for several tens, hundreds or thousands of years and thus could store large amounts of water, posing a potential threat to communities living downstream, sometimes hundreds of kilometres from the dam site. It can be exemplified by the catastrophic breach of a dammed lake in the upper reaches of the Rio Barrankos in Argentina (Hermanns et al. 2011), after which the flood travelled for about 1000 km before reaching the Atlantic Ocean. Studies of such features face difficulties due to their size, complexity and irregularity of internal structure. The presented case study relates to the investigation of the internal structure of a combined blast-fill and earth-fill dam of the Kambarata 2 Hydropower Plant (KHPP-2) and describes a set of geophysical tools and hydro-geomechanical analyses that could also be used to also assess the stability of (possibly much larger) natural dams. An application of similar methods to such a natural dam is presented in Torgoev et al. (2013).

The KHPP-2 is located on the Naryn River in Kyrgyzstan (Figure 1), and it is part of the Naryn hydropower cascade comprising six operating stations with a total capacity of approximately 3200 MW (see location in Figure 2). KHPP-2 is one of the smaller stations producing a power of 360 MW (when all three units are installed) and initially it was designed to be one within a group of three stations. Upstream from the Kambarata 2 reservoir the construction of at least one additional station is planned, with a total capacity of nearly 2000 MW.

The entire Naryn hydropower cascade is located in the seismically active Central Tien Shan (Abdrakhmatov et al. 2003), on both north-east and south-west sides of the large Talas-Fergana Fault strike-slip fault (see Figures 1 and 2). The design of the dams had to take into consideration the high seismic hazard (see Figure 2) marked by a Peak Ground Acceleration (PGA) of ~0.38 g for a 475 year period according to Abdrakhmatov et al. 2003, who used zones as seismic sources. For the same area, Bindi et al. (2012) obtained a PGA of ~0.28 g for a 475 return period – using mainly large active faults as seismic sources. The KHPP-2 dam stability was assessed for a maximum horizontal acceleration of 0.3 g, which is close the latest 475-year return period PGA of 0.28 g predicted by Bindi et al. (2012). Undoubtedly, also ground acceleration values with much larger return periods (>1000 years) should be considered for a complete seismic dam stability assessment. As part of a Master thesis (Lamair 2012) seismic hazard had been assessed for the Central Tien Shan for longer return periods (up to 10,000 years). Those calculations indicate a PGA of almost 1 g for the entire Central Tien Shan. For such long return periods the Talas-Fergana Fault zone is marked by a PGA of even more than 1 g, while it should be noted (Figure 2)

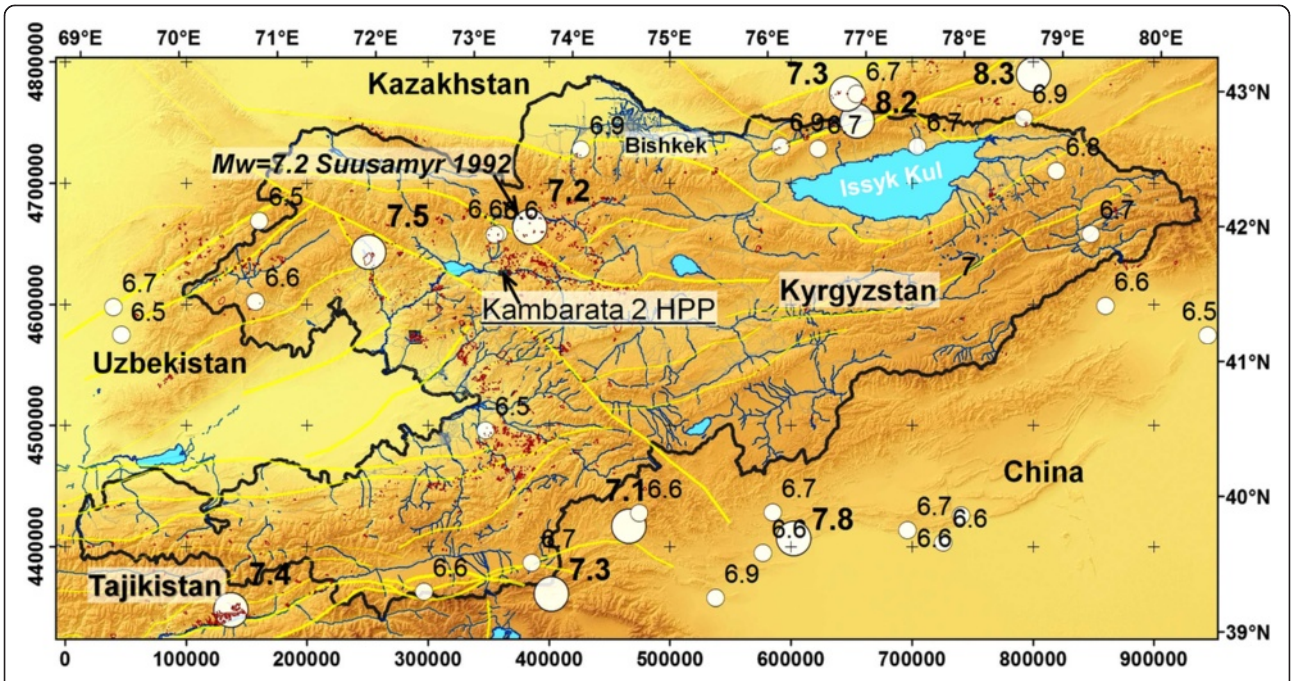

Figure 1 Map of Kyrgyzstan (with indication of geographic, upper and right axes as well as UTM43 N projection reference systems, lower and left axes) with location of KHPP-2 site, major historical earthquakes (circles) and faults (yellow), river network in blue and road network in grey; landslide locations are shown by red dots.

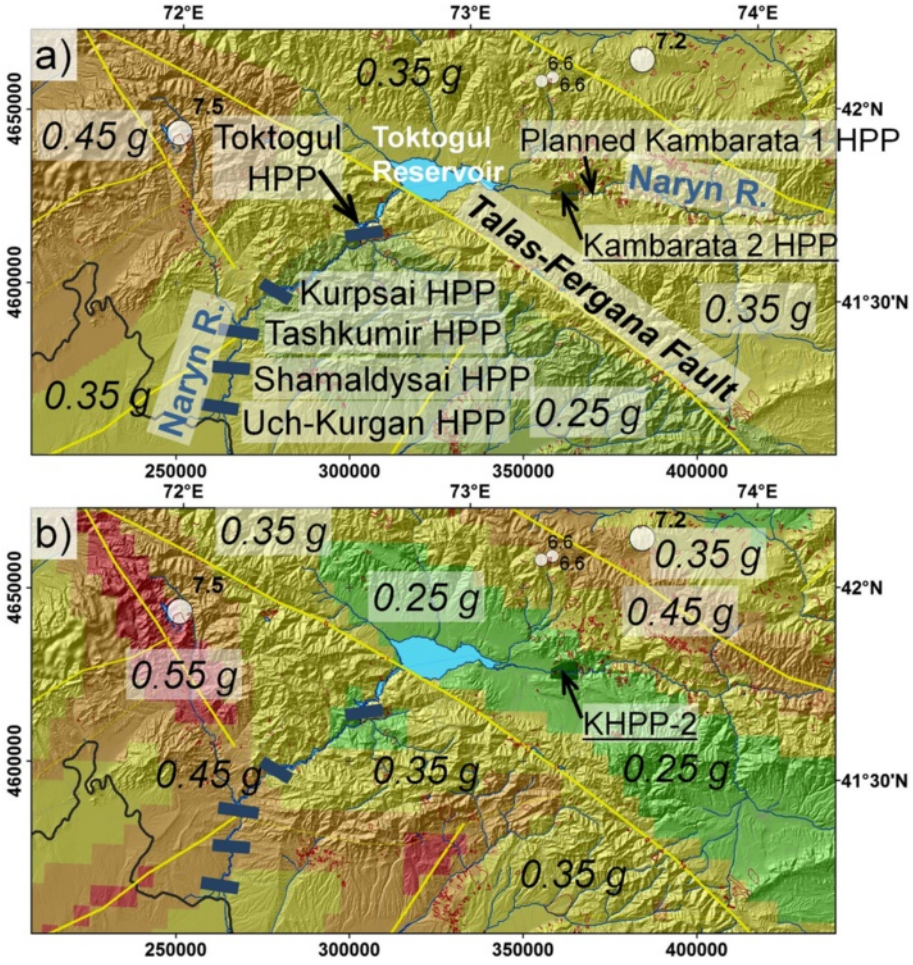

Figure 2 a) Seismic hazard map of the Central Tien Shan (Abdrakhmatov et al. 2003; with indication of geographic and UTM43 N projection reference systems,) showing the location of the Naryn HPP cascade and the presence of major active faults, including the largest one, the Talas-Fergana Fault. b) Seismic hazard map of the same area computed by Bindi et al. (2012). Landslide locations are shown by red outlines.

that acceleration values are not higher along this fault zone than for the surrounding area if the shorter standard return period of 475 years is considered (due to the large time intervals of several hundreds of years between characteristic major shocks occurring on each of the three segments of this fault, see Korjenkov et al. 2010). Here, the extreme PGA values for large return periods were not used for the seismic dam stability assessment as those values are affected by very high uncertainty; further, it will be shown that dam instability becomes critical even for the 475-year PGA values.

Possible impacts by landslide activation (through seismic shaking or reservoir filling) were not considered even though several landslides are known to have occurred near the dam site and in the reservoir area (known landslides are plotted on the maps in Figures 1 and 3, see also the image of two ancient large rockslides with an estimated volume of 10–20 10^6 m^3 in the KHPP-2 reservoir area). Here, only the stability of the dam itself has been computed on the basis of all information on the dam structure that could be compiled from various surveys.

The basal and central part of the KHPP-2 dam is made of an artificial mass movement that was created in December 2009 through an oriented blast (2600 tons of explosives that was distributed within two galleries as shown in Figure 4) of the right-bank rock promontory near the present upper part of the dam (snapshots of blast event, kindly provided by A. Obopol, are shown in Figure 5).

According to the design, the entire dam material should have been produced by blasted rocks with a volume of 3 10^6 m^3 and a height of at least 50 m. However, after the explosion only about two thirds of the planned dam volume was reached and an additional rock mass of 780,000 m^3 had to be moved (mostly from the explosion

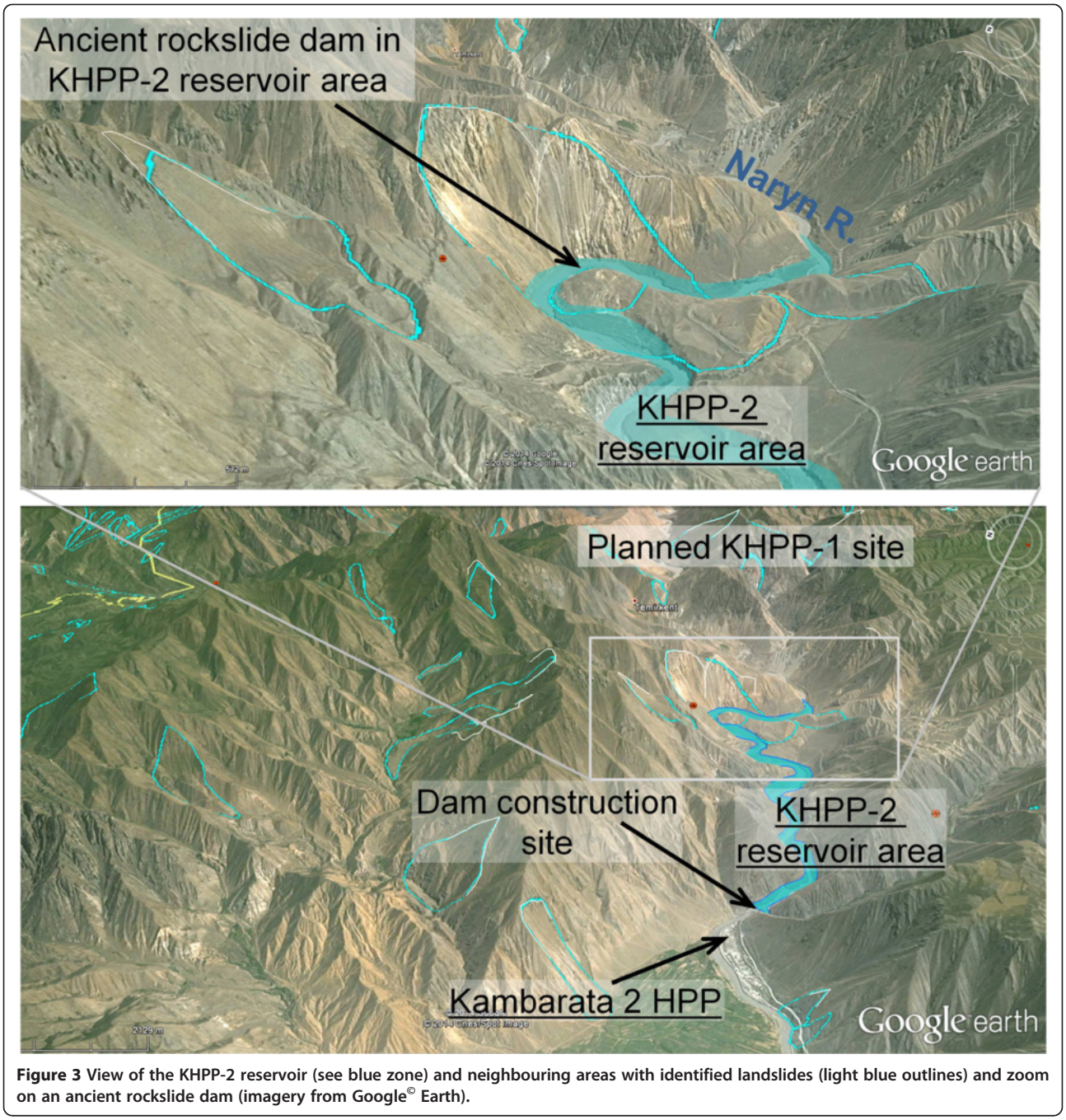

Figure 3 View of the KHPP-2 reservoir (see blue zone) and neighbouring areas with identified landslides (light blue outlines) and zoom on an ancient rockslide dam (imagery from Google© Earth).

area) to the site to fill the dam up to the design elevation of 961 m using traditional methods.

Blast-fill dams

Why was the Kambarata 2 dam designed as a blast-fill dam? This technology was mainly developed in the Soviet Union and in China; it was expected to be more cost-efficient than other dam construction methods, especially if applied in high (remote) mountain areas (Adushkin 2011). The most famous example is the Medeo dam that was constructed in the 1960s to protect the city of Alma Ata from debris flows: it actually did so in 1973 (Nedriga et al. 1978; Gerashnov et al. 1979). Other examples are the Baipaza HPP dam in Tajikistan (1968), the Ak-Su dam in Dagestan (1972), the Burlykia (1975) and Uch-Terek (1989) experimental dam in Kyrgyzstan and some others presented in Adushkin (2011). The Burlikya and Uch-Terek explosions were carried as tests for the Kambarata 1 dam construction.

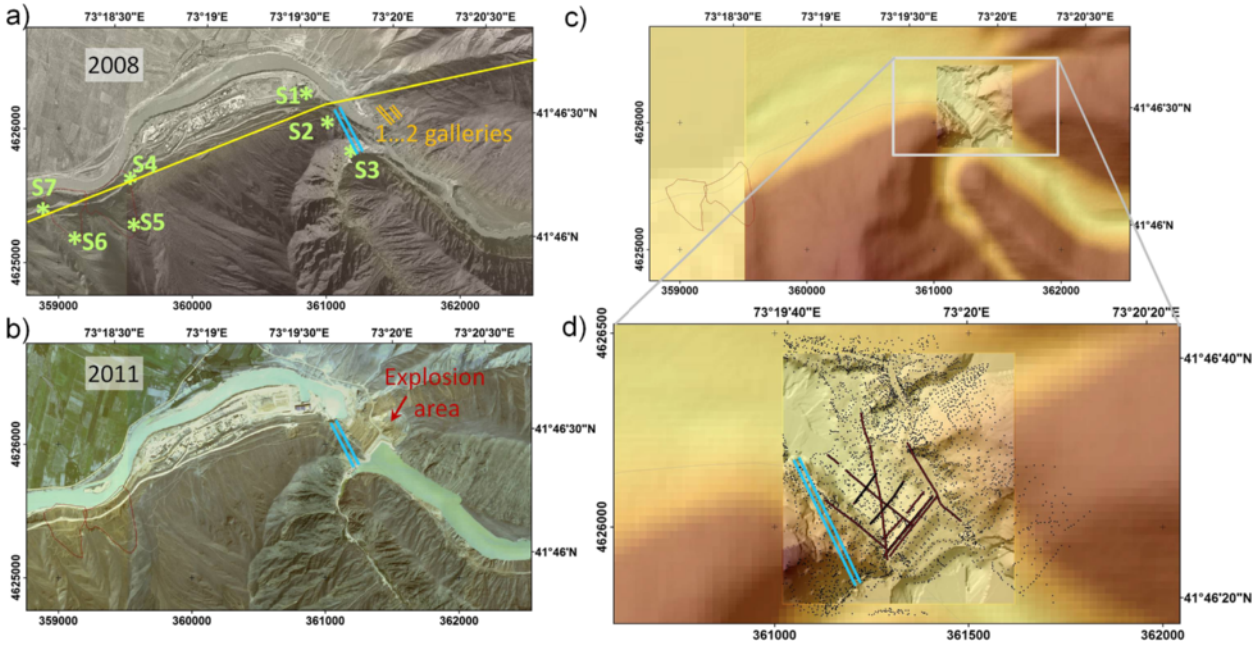

Figure 4 a) **Panchromatic Quickbird image (0.6 m resolution) of the dam site before blast (in 2008) with location of the local 'Southern Fault' (yellow line), seismic stations S1-S7 which recorded the blast and the two galleries that had been filled with explosives; underground spillway in blue. b)** Coloured Quickbird image (2.5 m resolution) of the dam site after complete shaping of the dam with location of explosion area (2011). **c)** Overlay of DEMs of the site: coarse 90 m SRTM DEM in the left part, 20 m SPOT DEM in the main part and local 2.5 m DEM constructed from total station measurements – see zoom with about 4500 topographic data points in dark blue in **d)**, together with locations of electrical resistivity profiles (violet lines).

Figure 5 The KHPP-2 explosion event on December 22, 2009 (11:54 am). a) Snapshots kindly provided by A. Obopol; note the slope failure near spillway exit caused by seismic shaking; see also title page of journal published in Bishkek on December 23, 2009 (title: 'Explosion of national importance'). **b)** Accelerograms recorded on the E-W and Z- components of station S2 above the spillway exit (location in Figure 4a).

Petrov et al. (1975) and Adushkin (2000, 2011) highlight the advantages of blast-fill dams compared to traditional rock-fill dams: blast-fill dams are generally less susceptible to inner erosion due to the presence of both fine- and very coarse-grained material created by the blast and they are considered to be more stable, especially in seismic conditions. Korchevsky et al. (2011) explain the latter characteristic through analogy with natural rockslide dams that proved to be very stable (using examples mainly from the Tien Shan) – probably also due to the mixture of fine- and coarse-grained material contributing to a larger resistance to friction when experiencing high amplitude shaking.

General information on KHPP-2 and the explosion event

The 60 m high KHPP-2 dam forms a blockage on the Naryn River resulting in a reservoir with a volume of 70 10^6 m^3 extending 10 km upstream from the dam. As the reservoir had filled up immediately after the explosion without the presence of a deviation of the river, the spillway had to be constructed beforehand within the rocks of the left bank of the Naryn River (opposite to the explosion area, see location in the maps in Figure 4, and view of the downstream exit in Figure 6 below). The maps in Figure 5 also show that one active fault crosses the site just downstream from the reservoir; near this so-called 'Southern Fault' two landslides had developed at a distance of about 2 km from the dam site. Along this Southern Fault evidence of recurrent Late Quaternary (likely Holocene) displacements with single-event offsets of 1–2 m each were observed.

Before the explosion, our team had participated in the setting up of a seismic monitoring network made of eight stations. Through this network, the seismic ground motions were measured in the near field of the blast (within a radius of 5 km). The locations of the seven nearest stations (one station was located at 5 km to the north of the site as reference) are shown in Figure 4a. Stations S1-S5 were equipped with accelerometers as the ground motions within a distance of 3 km from the blast were expected to be very high; the other stations were equipped with seismometers. Station S1 located on the first floor of the power house had produced the highest acceleration of about 1.8 g on the Z-component (this high amplitude was probably due to a resonance effect of the concrete floor); the highest acceleration on natural ground was obtained at station S2 above the spillway exit (near a triggered slope failure that can be seen in Figures 5a and 6d); the recorded accelerogram is shown in the lower right corner of Figure 5: the groups of waves related to the two sub-explosions in gallery 1 and 2 can be clearly identified. The largest amplitude

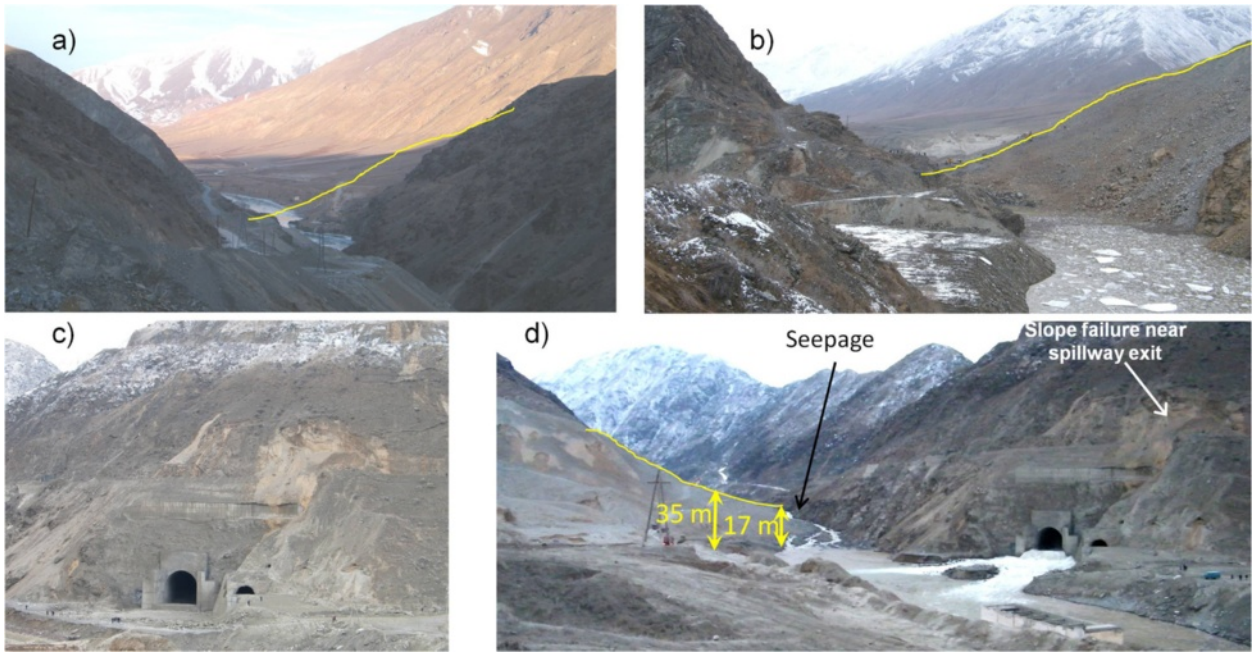

Figure 6 a) View towards the Kambarata canyon before the explosion (from upstream to downstream); the yellow line shows the approximate profile of the dam created by the blast. b) Similar view towards the blocked canyon a few hours after the blast. **c)** Spillway exit downstream from the dam 2 hours after the blast, without water outflow (note also the slope above the exit that partly failed during the explosion). **d)** View of the spillway exit and of the downstream side of the dam, one day after the blast (with water outflow, note also the seepage in the upper part of the dam due to insufficient height and thickness of the blockage reached during explosion).

is −1.02 g on the E-W component, i.e. oriented towards the west – due to the directivity of the blast.

For comparison, Figure 4 also shows the satellite image of the site after completion of dam construction in 2011 and the digital elevation models (DEM) available for the site.

As indicated above, the blast did not produce the designed dam height of at least 50 m above the river level. At the opposite slope (left bank), the dam crest was only 17 m above the river level and was at risk of overtopping as the upstream entry of the spillway is located nearly at a similar level (partly seen in Figure 6b). Intensive seepage was actually observed during the next few days, in parallel with the normal outflow through the spillway (see Figure 6d). Thanks to immediate filling of the missing material by bulldozers at the left bank side, the overtopping could be inhibited and the dam was finally saved. However, later measurements showed that this part remained the weakest within the dam structure (see investigation results below).

Filling works continued over several months and only in the summer of 2010 was the dam shaped as planned according to the design (see maps in Figures 4 and 7, see view in Figure 7). The dam now has a central crest height of 60 m (above river level) reaching an elevation of 961.0 m; the width along the crest is 230.5 m and along the middle part it is 444.5 m; the downstream slope was shaped with a slope of 1:2.5.

Methods

Several surveys have been carried out on the dam site since the explosion event. Most started when the design height and form of the dam had been reached at the end of 2010. A topographic survey was carried out by a local team (Design and Research Institute HYDROPROJECT, Kara-Kul), which had collected 4500 data points with a total station in 2010; those cover the entire dam site and surrounding areas (see small dark blue dots in Figures 4d and 7). These data points were interpolated by kriging to produce a 2.5 m resolution DEM of the site (shown above in Figures 4c and d); kriging of the data points had produced that best DEM result among the applied surface interpolation techniques, including triangulation and inverse distance weighting. In 2010, about 20 piezometers had been installed on and near the dam to control ground water levels (location shown in Figure 7 marked by light blue points).

The comparison of piezometer data collected (from September 2010 until September 2012) along the main dam section with the reservoir level (Figure 8) shows that the latter had a clear influence on the piezometric levels in the dam. This reveals that water infiltration had

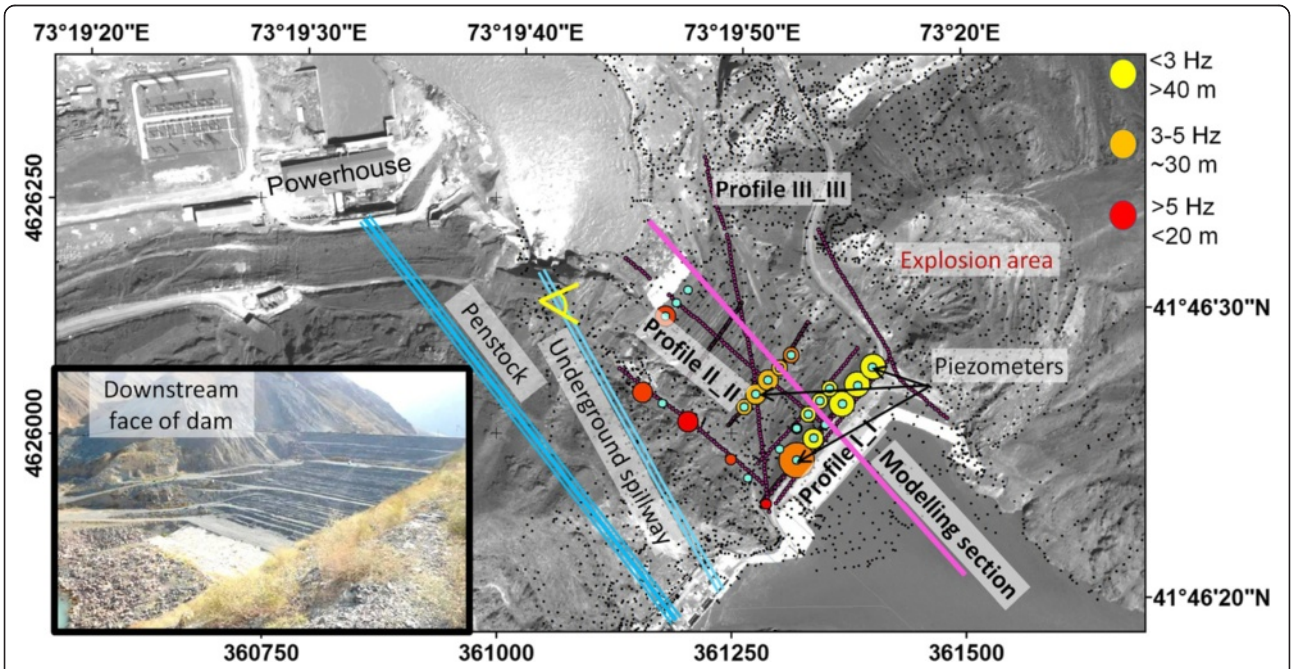

Figure 7 Panchromatic Quickbird image (0.5 m resolution) of the dam site after the blast (in 2011) with underground spillway and penstock shown by blue lines. Electrical tomography profiles are shown by dark violet point-lines (each point is the location of one electrode). H/V measurements are shown by coloured filled circles; colours according to measured resonance frequencies from 2.7 Hz in yellow (1D thickness of more than 40 m considering an average Vs ~500 m/s) to more than 5 Hz in red (1D thickness of less than 20 m for average Vs ~ 400 m/s; sizes of circles indicate the measured amplitude). Light blue dots show the location of piezometers. Dark blue dots are topographic measurements. Lower left corner: view of the downstream face of the dam made from the point marked by the yellow view angle.

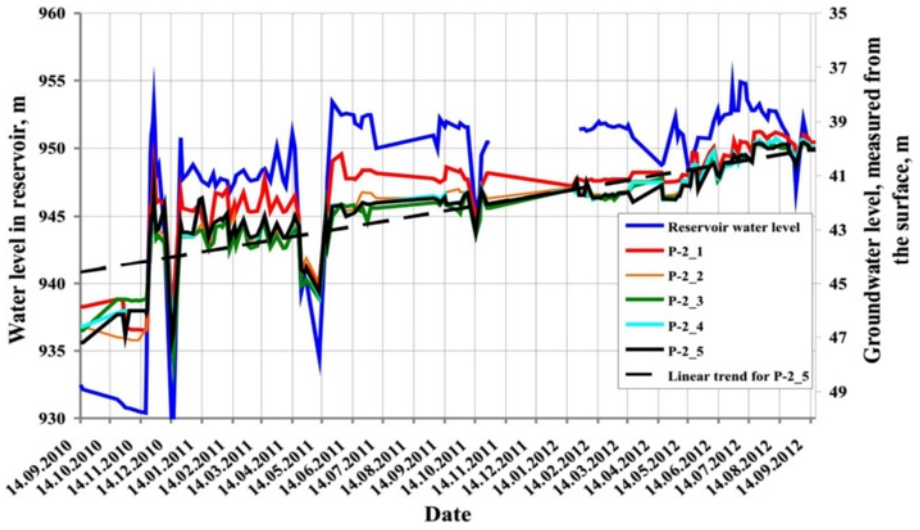

Figure 8 Graph showing the evolution of the water level in the piezometers compared with the reservoir level change from September 2010 until September 2012.

taken place during that period (before the final concrete screen was installed in the central part of the dam, but after construction of the clay screen that was obviously not sufficient to inhibit water inflow).

In order to get a more continuous image of the changing hydrogeological conditions within the dam structure, four 2D electrical resistivity tomography (ERT) surveys were carried out on the dam site, in July 2012, September 2012, June 2013 and September 2013. In 2012, also seismic refraction profiles had been completed by a local company (Engineering Prospecting Institute Kyrgyz GIIZ). Those provided quite ambiguous results that were not implemented in the final geophysical model. In parallel with the ERT survey in September 2012, also 20 ambient noise H/V measurements were completed (with a CityShark seismic station and a Lennartz 5 s seismometer) to provide information on the resonance frequency of the local site conditions. The selection of seismic and ambient noise measurements combined electrical resistivity profiles was based on our good experience with those methods on landslide sites (see, e.g., Danneels et al. 2008).

The HV results are shown in Figure 7 as circles coloured according to the measured fundamental resonance frequency f0 (yellow for f0 < 3 Hz up to red for f0 > 5Hz). The lowest frequencies (2.5-2.7 Hz) were measured on the dam crest near the centre and north-eastern part of the dam marked by the largest local dam thickness (about 50 m). As the thickness is known over the dam site, a simple equation linking the thickness 'h' of the soft material to f0 and the shear wave velocity 'Vs' (h = Vs/4/f0) allows us to make an estimate of Vs: Vs = h*4*f0, Vs = 50*4*2.5 ~ 500 m/s. Higher f0 was measured in the lower and lateral parts of the dam, which is in agreement with the decreasing thickness in those parts.

The extensive ERT surveys were completed with the GeoTom-MK1E100 RES/IP/SP equipment (GEOLOG2000 Company, Augsburg, Germany). They included between six and eight profiles that were installed in the same places in 2012 and 2013 along and across the dam. The longest ERT profile III_III (400 m length, penetration depth of about 70 m, see location in Figure 7) had been completed along a diagonal section crossing the downstream face of the dam from south to north. ERT profile II-II (300 m length, penetration depth of about 55 m) was installed along the central SE-NW section of the dam (shown together with dam section in Figure 9). Smaller ERT profiles (100–200 m, penetration depth of 20–35 m) had been installed along the dam crest (ERT profile I_I in Figure 10) and along bench terraces on the downstream dam face. All ERT profiles used the available 100 electrodes with a spacing adapted to the total length (4 m for the 400 m long profile, 1 m for the 100 m long profiles); measurements were made according to the Wenner-Schlumberger method. All ERT data were processed through 2D inversion with the Res2Dinv software.

ERT profiles I_I that were set up in July 2012 (Figure 10b), September 2012 (Figure 10c) and September 2013 (Figure 10d) along the dam crest show average resistivity values within the dam structure ranging from 150 Ω.m in the lowest and wet part of the dam to more than 3000 Ω.m near the surface of the dam covered by dry gravel (with maximum values in the north-eastern part near the explosion area). Lower resistivities (<500 Ω.m) had also been measured in July and September 2012 at a

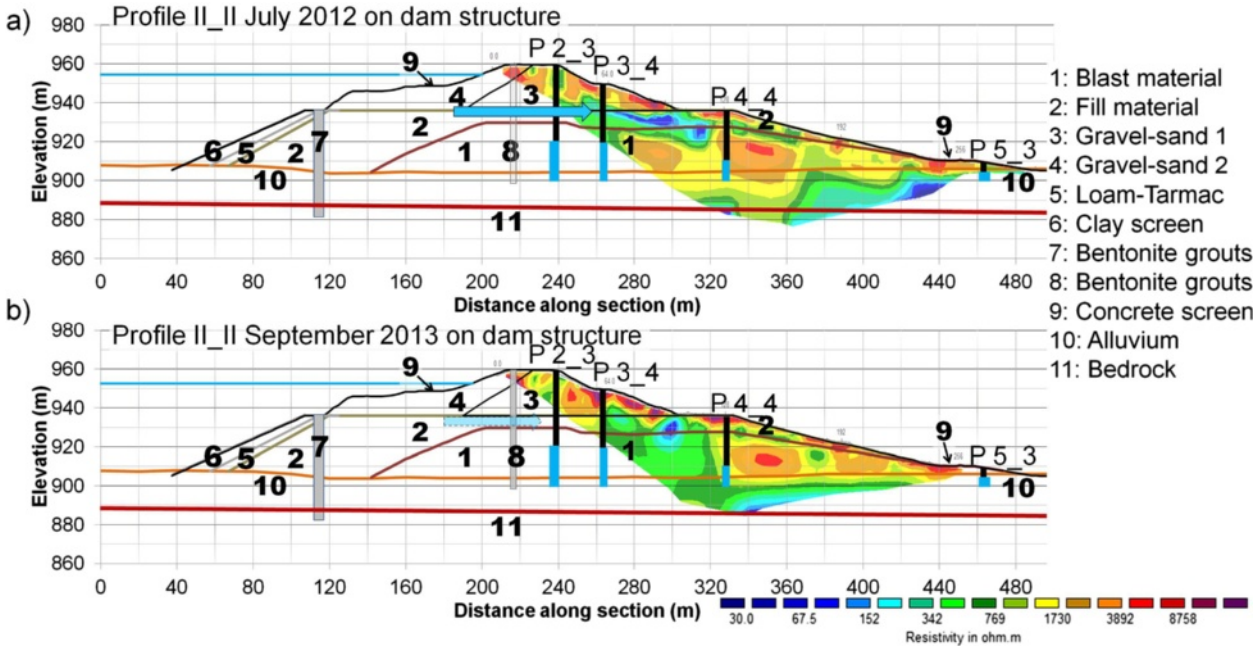

Figure 9 a) **Dam structure (and composition – numbered materials are listed in the right legend) defined on the basis of available data and schemes with overlaid piezometers of the central axis and electrical resistivity profile II_II measured in July 2012. b)** Dam structure compared with ERT profile II_II measured in September 2013. Note the increased resistivity in the central-left part of profile II_II in September 2013, probably due to reduced water flow (represented by blue arrow) through the dam (bentonite grouts '8' had been enhanced in summer 2013).

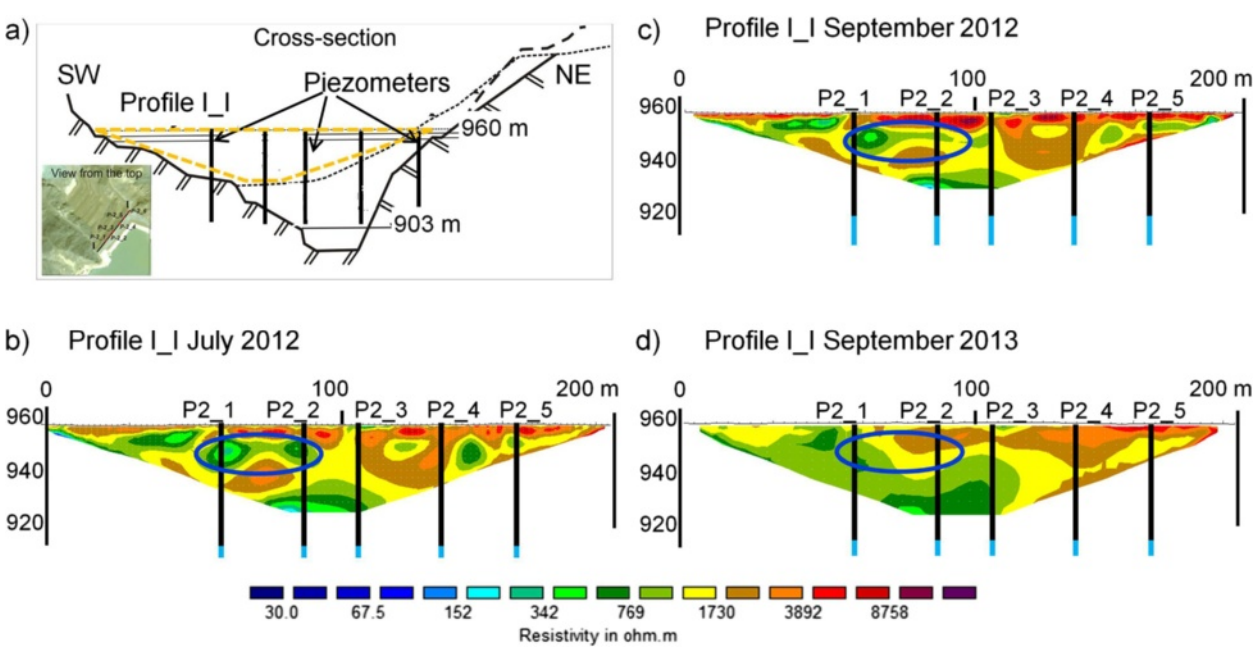

Figure 10 a) **Schematic cross-section with piezometer and ERT profile I_I location (orange dashed outline) along dam crest. b)** ERT profile I_I measurements shown for July 2012; **c)** for September 2012; **d)** for September 2013, together with water levels in piezometers located along the profile. See also blue outline of possible piping zone that disappeared after new grouting along the crest in summer 2013.

depth of about 10 m in the south-western part of the dam (blue oval outline in Figures 10b, 9c, 9d). Those lower values had been attributed to possible water piping.

Below, in Figure 9, ERT profile II_II is overlaid with the dam structure. The data used for establishing this cross-section had been compiled from several sources (mainly provided by Design and Research Institute HYDROPROJECT, Kara-Kul). The core part represents the blast material (1) covered by the material filled immediately after the blast event (2, mainly moved from the blast site). On top, the dam crest is composed of gravel-sand material (3, 4) with uncertain composition and structure. One loam-tarmac (5) and one clay layer (6) cover the lower upstream face of the dam. In this part, bentonite grouting had been completed (7). Additional bentonite grouts were injected along the dam crest (8). Concrete screens were installed both on the up- and downstream faces (9). The whole dam lies on top of 10–15 m of alluvial sediments (10) that had not been removed before the blast event and the bedrock (11).

On the ERT profile II_II of July 2012 along the section shown in Figure 9a, it can be seen that the lowest resistivities of less than 100 Ω.m appear within the fill material while the underlying blasted material has clearly higher resistivities of more than 200 Ω.m, and in many places even above 1000 Ω.m. The highest resistivities were measured within the gravel-sand material composing the dam crest indicating that no water infiltration occurred in the upper part, even when the reservoir level was near its maximum, probably due to the strong screening by the concrete plates (material 9 on the upstream face). Low resistivities within the fill material can be associated with water inflow below these plates due to insufficient compaction of the post-blast filling. On the basis of the combined observation of piping below the crest and water inflow in the fill material, we recommended an enhancement of the bentonite grouting below the dam crest. This was completed in summer 2013. The test ERT survey in September 2013 showed that this additional measure apparently had reduced the water inflow as clearly higher resistivities were observed within the former piping zones below the crest (Figure 10d) marked now by medium resistivity of more than 500 Ω.m and within the fill material along the main section (Figure 9b). However, it can be noted that those additional measures do not seem to have had any influence on the piezometer levels (see Figure 9).

Results and discussion

Modelling

All geophysical profiles and soundings were compiled on a GIS platform (map views are shown in Figures 4 and 7). The data located in the central part of the site containing the dam structure were then formatted for representation in a 3D model created with GOCAD software (version 2009.2). The results presented here are based on a Master's thesis that was completed by Xu (2014). This work has also shown that a refitting of the positions of some profiles or soundings was necessary in order to get a coherent 3D data set. The main references used were the piezometer heads installed along the dam crest.

The most extensive data sets are the ERT profiles and the 2.5 m DEM of the site. Combining geophysical, geotechnical and structural information, three distinctive contacts were defined and digitized on the profiles composing the 3D model (see dotted lines in Figures 11a and b). The lowest contact marks the top of the low resistivity zone in the alluvium and bedrock (red dots in Figures 11a and b); the middle contact (green dots in Figures 11a and 10b) indicates the limit between the blasted rocks and the wetter and probably less compacted fill material; the upper contact (yellow-golden dots in Figures 11a and b) marks the basis of the very dry and highly resistive gravels. These contacts do not exactly follow the design structure but are considered to better reflect the actual geomechanical-hydrogeological situation that is more relevant for groundwater flow and slope stability modelling.

Contacts of the same type were then interpolated to form surfaces (Figure 11c). Between the surfaces, the volumes were filled to create a solid model (Figure 11d): the blue solid represents the low-resistive alluvium and top of bedrock, the yellow-orange solid is mainly composed of blast-fill with medium resistivities, the green solid combines low-resistive fill and gravel-sand material, the reddish solid on top of the latter marks the highly resistive (dry) gravels deposited on top of the dam structure.

The central section across this model is overlaid with the dam structure in Figure 12a. Here, it can be seen that the contacts do not exactly follow the limits of the designed dam structure. In particular the basis of the gravel-sand material '3' is at a clearly lower level than the digitized basis of the highly resistive dry gravels. This is due to the fact that the lower part of material 3 has medium resistivities; those may be attributed to a wetness that could only build up in finer (sandy) material which would be similar to the underlying fill.

Both, the geophysical and the design structure model were then combined to create the numerical model shown in Figure 12b. This model was created with the GGU software package developed to assess geoengineering problems. The hydrogeological and geomechanical properties (here, only the shear resistance was considered) of the modelled materials are presented in Table 1. They were determined through laboratory

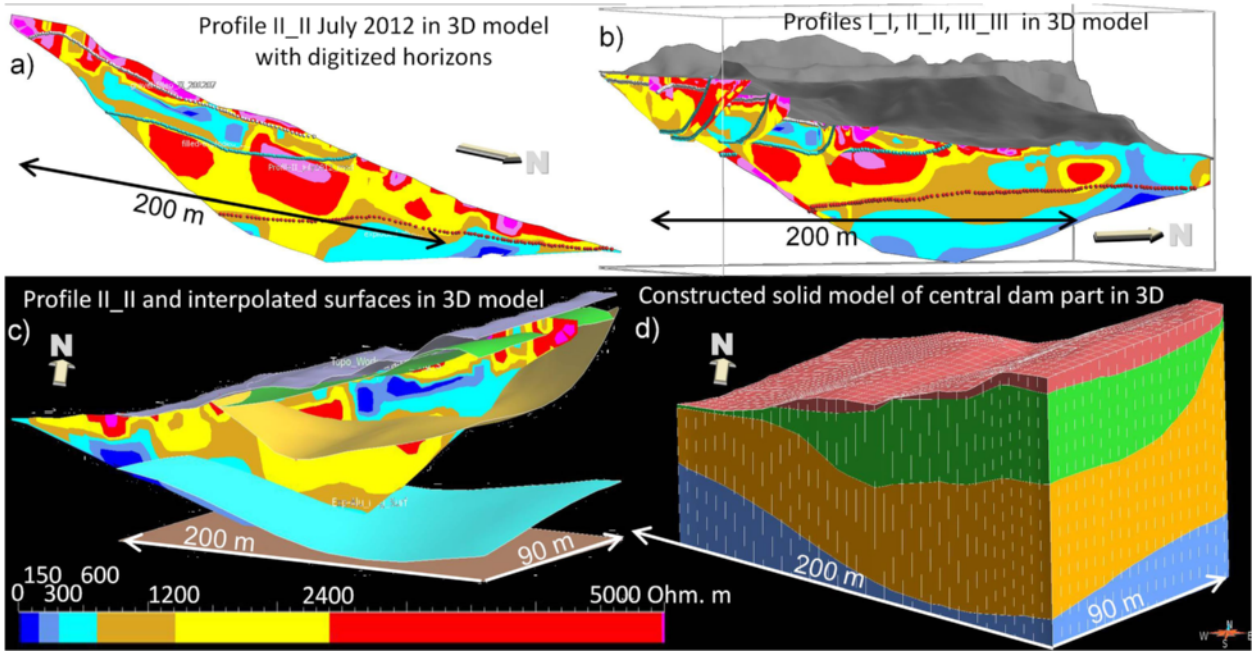

Figure 11 Electrical resistivity profiles and topographic surface data imported in the GOCAD software to build a 3D model. a,b) Digitisation of distinctive resistivity levels. **c)** Creation of surfaces through interpolation of the same digitized resistivity levels. **d)** Creation of a solid model from interpolated surfaces (material filling between surfaces).

tests applied to samples extracted from the piezometer boreholes and from other parts of the dam.

Firstly, modelling was performed with the GGU-SS-FLOW2D program based on numerical simulations with finite elements to calibrate the relatively uncertain hydraulic conductivity coefficients Kf (values provided by the Design and research Institute HYDROPROJECT, Kara-Kul). This calibration was controlled by the piezometric levels measured along the main dam section (see blue level at P2_3, P3_4, P4_4 and P5_3 in Figure 12a).

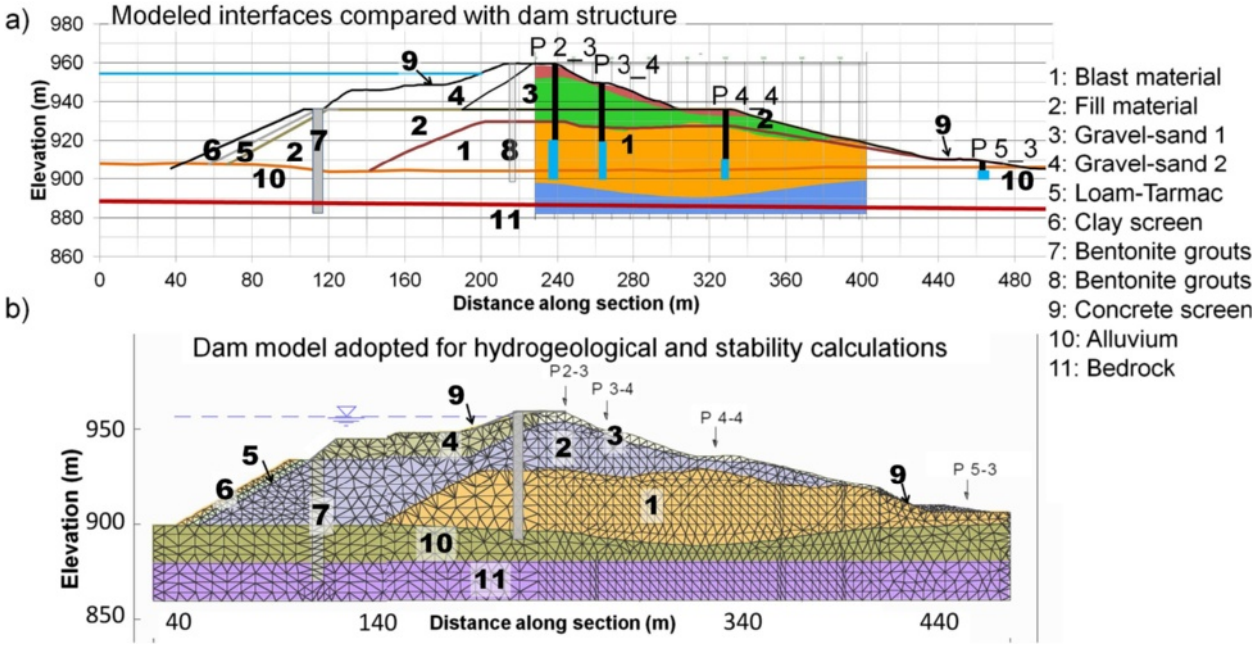

Figure 12 a) Initial dam profile corrected on the basis of the main section obtained from the 3D model constructed in GOCAD. b) Finite-element model built on the basis of the corrected 2D section of the dam.

Table 1 Dam material properties used for hydrogeological and slope stability modelling

Material	Hydraulic conductivity coeff. Kf initial (m/s)	Hydraulic conductivity coeff. Kf calibrated (m/s)	Cohesion C (kN/m2)	Internal Friction angle Φ (°)	Specific weight γ (kN/m3)
1: Blast-fill	$4\ 10^{-3}$	$3\ 10^{-5}$	200	38	20
2: Fill	$3\ 10^{-3}$	$3\ 10^{-4}$	20	30	20
3: Gravel	$8\ 10^{-4}$	$8\ 10^{-4}$	50	40	22
4: Gravel-sand	$8\ 10^{-4}$	$1\ 10^{-6}$	50	40	22
5: Loam-Tarmac	$1\ 10^{-5}$	$1\ 10^{-5}$	30	28	20
6: Clay layer	$1\ 10^{-8}$	$1\ 10^{-8}$	30	28	20
7-8: Bentonite grouts	$1\ 10^{-10}$	$1\ 10^{-10}$	30	28	20
9: Concrete screen	$1\ 10^{-10}$	$1\ 10^{-10}$	300	40	24
10: Alluvium	$1\ 10^{-3}$	$8\ 10^{-5}$	30	28	20
11: Bedrock	$4\ 10^{-3}$	$1\ 10^{-9}$	300	40	24

Note: Bentonite grouts 8 were not modelled due to missing detailed data. Above values are assumed according to data known for bentonite grouts '7'.

With the initial Kf-values, the modelled groundwater levels were much higher than those known from the piezometers. Actually, Figure 13a shows that the whole dam would be 'flooded' if the Kf-values were as high as previously estimated. Therefore, Kf-values were iteratively decreased in order to model water levels within the dam that corresponded to those observed. Through this modelling it was revealed that the most critical values were associated with the gravel-sand material 4 and the blast-fill material 1. In fact, the Kf-value of material 4 had to be decreased from $8\ 10^{-4}$ m/s to $1\ 10^{-6}$ m/s in order to avoid water inflow in the upper part of the dam that has never been observed. Furthermore, the Kf-value of the blast-fill material was decreased by a factor of more than 100 from $4\ 10^{-3}$ m/s to $3\ 10^{-5}$ m/s to create the larger observed groundwater level gradient within the dam (compare graph b with c in Figure 13). In this regard, it should also be noted that the Kf-values of the bedrock had to be strongly decreased from $4\ 10^{-3}$ m/s to $1\ 10^{-9}$ m/s, otherwise water flow under the dam and under the bentonite grouts 7 would have been able to create much higher piezometer levels (than those observed) in the

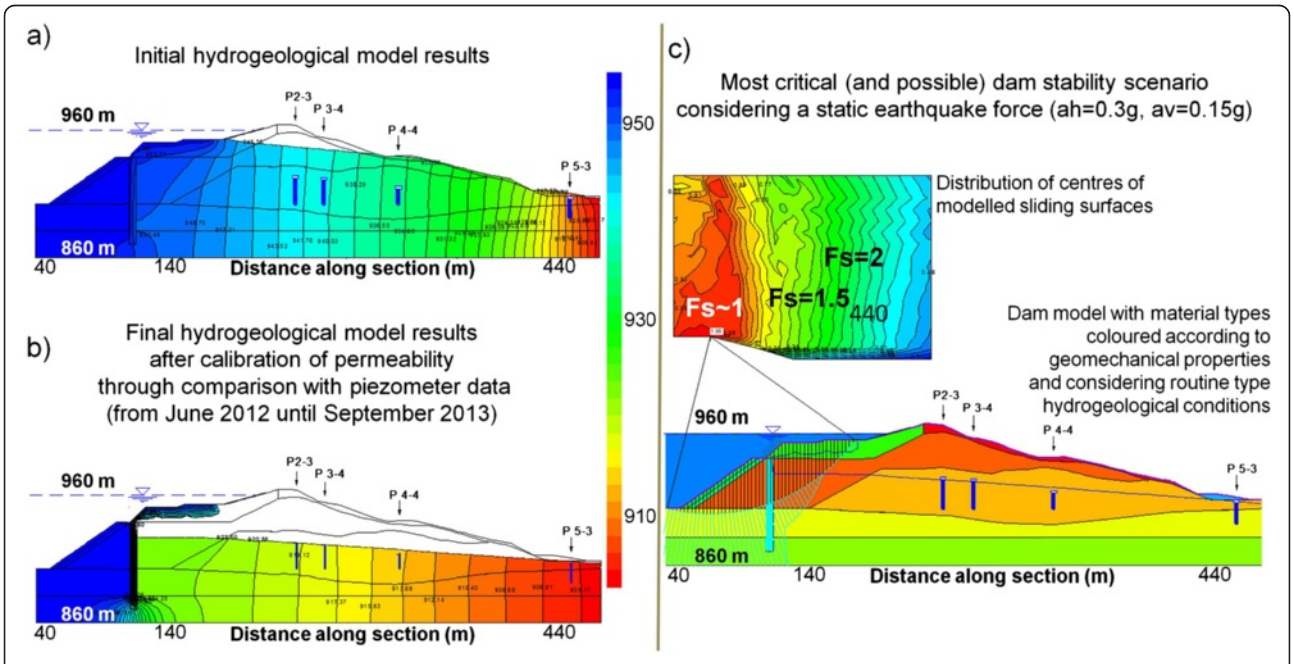

Figure 13 Hydrogeological models with (a) initial parameter Kf-values (above, provided by local company and engineers) and (b) with Kf-values calibrated through comparison of modelling results with piezometer levels measured in July 2012 and September 2013. c) Calculated dam stability scenario (most critical one among realistic scenarios) using average water level in the dam and reservoir and considering seismic effects: horizontal acceleration of 0.3 g and vertical acceleration of 0.15 g.

downstream part of the dam. With these much lower Kf-values, a very strong piezometric gradient appears in the bedrock under screen 7, which is likely to be a realistic situation (compare gradient in the lower left part of Figure 13b with the same location in Figure 13a) as evidenced by the low piezometer levels on the downstream face.

Interestingly, the Kf-values of the alluvium also had to be decreased by a factor of 12 to obtain results comparable with the observations, while the values were well constrained by hydraulic conductivity measurements that had been performed on alluvium material before dam construction. Actually, it is likely that these values decreased when the material was compacted under the load of the dam (especially during the blast event). Nevertheless, according to all modelling results obtained after calibration, highest groundwater flow velocities were obtained in the alluvium material.

Furthermore, we believe that clogging related to deposition of fine material transported by water infiltrating the dam during the first two years contributed to the reduced Kf-values in most dam materials and the underlying alluvium.

Various reservoir level scenarios and associated hydrogeological conditions were then used as inputs for slope stability calculations with the GGU-STABILITY software that implements classical static as well as pseudo-static methods allowing us to include seismic loads. One recent application of this program to seismic slope stability calculations can be found in Koltuk and Fernández-Steeger (2014).

The most critical scenarios under static conditions (factor of safety $Fs <= 1$) that were modelled include: local or general slope instability on the upstream face, during rapid or total reservoir discharging (due to large slope gradients, missing counterbalance of water load, and remaining pore pressures in the dam in the case of rapid discharge); and total instability of the downstream face if the dam is overtopped during flooding (due to water infiltration on the downstream face and related increased pore pressures). Such situations should be avoided and actually could be controlled, especially the one of total discharge which should be almost impossible due to the elevated location of the spillway entry.

The same scenarios are logically also unstable if a seismic load of $Ah = 0.3$ g on the horizontal component and $Av = 0.15$ g on the vertical component is included – these values are based on the seismic hazard estimates for this region for a 475-year return period (as presented above). The combinations of extreme hydrological and severe seismic conditions needed are extremely unlikely, but not impossible (besides the one of total discharge). The most realistic critical scenario that could lead to instability is shown in Figure 13c: the upstream face would be only marginally stable for common hydro(geo)logical conditions if impacted by the 475-year return period seismic load of $Ah = 0.3$ g and $Av = 0.15$ g.

It is important to note that these 2D computations do not reflect the total hydrogeological and geomechanical behaviour of the 3D dam structure. In particular, it could be that the weaker western part of the dam exhibits less favourable hydrogeological characteristics combined with lower slope stability. However, this weakness may be compensated by the proximity of the stronger bedrock. These issues can only be treated within a full 3D model analysis which is beyond the scope of our relatively limited assessment.

Conclusions

In this paper, a case study is presented that combined investigation and modelling of the blast- and earth-fill dam of Kambarata 2 HPP in the Central Tien Shan, Kyrgyz Republic. The blast event of December 22, 2009 had been recorded both by accelerometric and by seismometric instruments. Related measurements showed that accelerations of about 1 g affected the slope opposite to the explosion site and that the vertical acceleration in the powerhouse was close to 2 g (but without causing significant damage). However, the blast cannot be considered as totally successful as the design height of the blast-fill of about 50 m above river level had not been reached. Consequently, immediately after the blast, earth material had to be transported from the explosion site to the opposite flank to rapidly increase the dam crest height in order to avoid overtopping. In 2010, additional works were carried out to complete the dam construction. Bentonite grouts were installed in parts of the upstream face and along the dam crest, over the entire dam height. These were added following recommendation by some of the authors because our geophysical monitoring had provided evidence of piping across the dam. During the geophysical survey completed in September 2013, after the additional bentonite grouting near the dam crest, clearly higher resistivities had been measured in the same places, which was likely to be related to the reduced groundwater flow across the dam. The geophysical surveys further showed that the blast-fill material, representing about 75% of the total dam volume, is characterized by relatively high resistivities (>500 Ω.m) and medium seismic velocities (S-wave velocity of about 500 m/s). These properties indicate a good compaction of the blast-fill material that contrasts with the lower quality of the earth fill that had been added on top of the rocks produced by blasting.

All topographic, geophysical and piezometric data from the dam site was compiled within a 3D geomodel constructed with GOCAD software. This kind of 3D reconstruction firstly allowed us to check more carefully

the coherence between data in three dimensions. Secondly, the 3D data were compared with the design structure of the dam in order to define the upper limits of the underlying alluvium, the deposited blast fill, earth fill and top gravel materials (represented by the dam surface). This comparison showed that the design shapes of composing materials were not all reflected by geophysical contrasts. We therefore combined both design structure and measured geophysical information in order to redefine material limits within a central volume. Thirdly, these limits were determined on each ERT profile and then interpolated to create surfaces representing the upper limits of the dam materials and underlying alluvium. Fourthly, from these surfaces a 200 m long, 90 m wide (along the crest of the dam) and 80 m high 3D model of the central and downstream part of the dam was built. This model contains the highest density of information from geophysical and piezometric measurements available.

The central cross-section of this model was extrapolated over the full profile of the entire dam and adapted in order to be compatible with all input data. This profile is composed of eleven sectoral parts made of nine different materials. Initial estimates of the permeability of the materials were used for hydrogeological modelling of groundwater flow through the dam. Comparison with piezometric data showed that the estimated hydraulic conductivities of most materials were too high; the low piezometric levels especially indicate that the materials composing the upstream face as well as the alluvium and blast-fill material must be characterized by low to very low permeability. The permeability of the two latter materials might have been caused by the compaction during the blast event (related to the high fall of the blasted rock and earth material).

On the basis of the calibrated hydrogeological model and the known geomechanical properties of the materials, dam stability calculations were completed for different scenarios considering different reservoir levels and varying seismic conditions. The unlikely (and almost impossible) cases either of totally empty or of an overtopping reservoir produced the lowest factor of safety, respectively, for the upstream and downstream faces. The possible case of a seismic load of $ah = 0.3$ g, $av = 0.15$ g impacting the dam under routine conditions could also cause its partial instability.

This case study can also be used as example for surveys on much larger natural – landslide or moraine – dams (such as applied by some of the authors on landslide dams in the Tien Shan, see for example Torgoev et al. 2013). The ERT method can be adapted to a dam of any size, as long as the profiles are long enough (investigation depth ~ 1/6 of the ERT profile length). The microseismic method is particularly suitable for prospecting deep sites; the investigation depth depends on site conditions (e.g., the thickness of soft material) and on the resonance frequency of the seismometer (the Lennartz 5 s seismometer used for this survey could be employed as well for natural/artificial dams with a thickness up to 500 m, considering an average S-wave velocity of 500 m/s for the dam material). Another promising tool to investigate large natural blockages would be the TEM or TDEM (Transient or Time-Domain Electro-Magnetics) technique. This method would provide particularly valuable results if the dam material presents relatively high resistivities and lies on less resistive alluvium or if groundwater flow occurs in the lower parts of the dam. The topographic measurements are not directly dependant on the size of the dam but rather on the sight conditions: here, a total station (theodolite) was used that requires a clear view between station and reflector; this is generally less restrictive than the unobstructed path needed between a differential GPS instrument and satellite. Certainly, for constructing a digital elevation model of the dam, classical photogrammetric or other remote sensing techniques could also be applied.

As a general conclusion, it was noted that this case study can be used as an example for surveys on much larger natural – landslide or moraine – dams. A series of geophysical methods (e.g., electrical and electro-magnetic techniques, seismic and microseismic measurements) can be applied to investigate even very deep dam structures. These methods have the advantage over classical direct prospecting techniques, such as drilling, of using equipment that is much lighter and thus more easily transportable and applicable in difficult terrain. Furthermore, they can provide continuous information over wider areas. This specific application to a blast-fill dam allows us to better outline the strengths and weaknesses of the exploration types and geomodels as a series of investigated parameters can be verified more easily than for natural dams.

Abbreviations

KHPP-2: Kambarata 2 Hydropower Plant; ERT: Electrical Resistivity Tomography; DEM: Digital Elevation Model; H/V: H over V ambient noise method; TEM/TDEM: Transient/Time-Domain Electro-Magnetic method.

Competing interests

The authors declare that they have no competing interests.

Authors' contributions

The authors HBH, IT, AT, AS completed the field investigations, HBH + YX + TFS completed the modeling part. All authors read and approved the final manuscript.

Acknowledgements

The Electrical tomography equipment was provided within the frame of NATO Science for Peace project LADATSHA, SFP983289. The same project had also funded the field work completed in connection with the blast event. We thank Engineering Prospecting Institute Kyrgyz GIIZ and the Design and research Institute HYDROPROJECT, Kara-Kul, for having provided valuable data. We also thank A. Obopol for having kindly provided the images of the Kambarata 2 blast of December 22, 2009.

Author details
[1]Department of Geology, University of Liege, Liege, Belgium. [2]Institute of Geomechanics and Development of Subsoil, Acad. of Sciences, Bishkek, Kyrgyzstan. [3]Geodynamics Research Center, JSC Hydroproject Institute, Moscow, Russia. [4]PowerChina Chengdu Engineering Corporation, Huanhua Nord Str. 01, 610072 Chengdu, China. [5]Department of Engineering Geology and Hydrogeology, RWTH Aachen University, Aachen, Germany.

Received: 15 December 2014 Accepted: 24 March 2015
Published online: 23 April 2015

References

Abdrakhmatov K, Havenith HB, Delvaux D, Jongmans D, Trefois P (2003) Probabilistic PGA and arias intensity maps of Kyrgyzstan (Central Asia). J Seismol Soc Jpn 7:203–220

Adushkin VV (2000) Explosive initiation of creative processes in nature. Fizika Goreniya i Vzryva 36(6):21–33

Adushkin VV (2011) Russian experience with blast-fill Dam construction. In: Evans SG (ed) Natural and artificial rockslide dams. Springer, Berlin, Heidelberg, Lecture Notes in Earth Sciences, pp 595–616

Bindi D, Abdrakhmatov KY, Parolai S, Mucciarelli M, Grunthal G, Ischuk A (2012) Seismic hazard assessment in central Asia: outcomes from a site approach. Soil Dyn Earth Eng 37:84–97

Danneels G, Bourdeau C, Torgoev I, Havenith HB (2008) Geophysical investigation and numerical modelling of unstable slopes: case-study of Kainama (Kyrgyzstan). Geophys J Int 175:17–34

Gerashnov GB, Zinevich YN, Shapovalov GI (1979) The Medeo mudflow-protection dam. Gidrotekhnicheskoe Stroitel'stvo 9:44–48

Hermanns RL, Folguera A, Penna I, Fauqué L, Niedermann S (2011) Landslide Dams in the Central Andes of Argentina (Northern Patagonia and the Argentine Northwest). In: Evans SG SG et al (eds) Natural and artificial rockslide dams. Springer, Berlin, Heidelberg, Lecture Notes in Earth Sciences, pp 147–176

Koltuk S, Fernández-Steeger TM (2014) Evaluation of seismic stability of coherent landslides: analytical approach versus FEM. In: Grützner, C. et al (eds) 5th International INQUA meeting on paleoseismology. Active Tectonics and Archeoseismology, Busan, Korea, pp 135–140, doi:10.13140/2.1.1815.9364

Korchevsky VF, Kolichko AV, Strom A, Pernik LM, Abdrakhmatov KE (2011) Utilisation of data derived from large-scale experiments and study of natural blockages for blast-fill Dam design. In: Evans SG SG et al (eds) Natural and artificial rockslide dams. Springer, Berlin, Heidelberg, Lecture Notes in Earth Sciences, pp 617–637

Korjenkov AM, Bobrovskii A, Mamyrov EM (2010) Evidence for strong Paleoearthquakes along the Talas-Fergana Fault Near the Kök-Bel Pass, Kyrgyzstan. Geotectonics 44(3):262–270

Lamair L. (2012) Calcul de l'aléa sismique pour une région dans le Tien Shan Central, étude in situ et modélisation dynamique de la réponse sismique de sites de bassin de retenue. Master Thesis, University of Liege

Nedriga VP, Pokrovskii GI, Korchevsky VF, Petrov GN (1978) Full-scale investigations of seepage in an experimental blast-fill dam. Gidrotekhnicheskoe Stroitel'stvo 7:21–24

Petrov GN, Reifman LS, Khusankhodzhaev FZ (1975) Dam construction by blasting. Gidrotekhnicheskoe Stroitel'stvo 10:15–19

Torgoev A., Lamair L., Torgoev I., Havenith H.B. (2013) A Review of Recent Case Studies of Landslides Investigated in the Tien Shan Using Microseismic and Other Geophysical Methods. In: Ugai K et al. (eds) Earthquake-Induced Landslides, Springer-Verlag Berlin Heidelberg 285–294

Xu Y. (2014) Geologische 3D Modellierung und Analyse der Standsicherheit des Kambarata-2 Sprengschuttdammes. Master Thesis, RWTH Aachen University